The Effect of Seismic Sequences in Probabilistic Seismic Hazard Analysis

Article *in* Bulletin of the Seismological Society of America · March 2022

DOI: 10.1785/0120210208

CITATIONS
23

READS
746

5 authors, including:

Nevena Sipcic
RED Risk Engineering + Development, Pavia
12 PUBLICATIONS **50** CITATIONS
SEE PROFILE

Mohsen Kohrangi
RED Risk Engineering + Development, Pavia, Italy--- https://www.redrisk.com/
77 PUBLICATIONS **1,574** CITATIONS
SEE PROFILE

Athanasios N. Papadopoulos
Moody's RMS
24 PUBLICATIONS **309** CITATIONS
SEE PROFILE

Paolo Bazzurro
University School for Advanced Studies - IUSS Pavia
166 PUBLICATIONS **7,165** CITATIONS
SEE PROFILE

The Effect of Seismic Sequences in Probabilistic Seismic Hazard Analysis

Nevena Šipčić*[1], Mohsen Kohrangi[2], Athanasios N. Papadopoulos[3], Warner Marzocchi[4], and Paolo Bazzurro[1]

ABSTRACT

Traditionally, probabilistic seismic hazard analysis (PSHA) considers only mainshock events and models their temporal occurrence through a homogeneous Poisson process. Thus, it disregards foreshocks and aftershocks, assuming they have a minor effect on PSHA. However, recent earthquake sequences, such as those in 2016–2017 in Central Italy and 2010–2011 in Christchurch, New Zealand, exposed the shortcomings of such a universally used but unconservative approach. Our efforts to quantify the bias in seismic hazard and risk estimates follow from these considerations. Herein, we investigate the epidemic-type aftershock sequence (ETAS) model's ability to reproduce the statistical features of long-term historical seismicity in Italy in two different regions. In addition, we calculate and compare the seismic hazard at two sites in Central Italy using different approaches: (1) with seismicity clustering modeled using the ETAS model; (2) with only mainshocks modeled by means of the Poissonian approach; and (3) with seismicity clustering modeled via a combination of Poisson and modified Omori law. We consider two cases: (1) the "unconditional case," which uses years of varying seismicity as initial conditions and, therefore, can be considered as a tool for predicting the long-term average hazard, and (2) "conditional case," in which the hazard is estimated after a specific period, in our case higher than average seismicity. We scrutinize the different modeling assumptions during the process and investigate the effect of using different declustering methods in Poisson-based models. As expected, we find that using the mainshock-only seismicity models yields lower hazard estimates compared to those obtained with the Omori and ETAS model. In addition, we show that Omori and ETAS model predict similar results in the unconditional case, but the Omori model considerably underpredicts the hazard in the conditional case, for a site close to the sequences, when temporal variations in seismic hazard are accounted for.

KEY POINTS

- This article addresses the effects of clustered seismicity in PSHA and compares different modeling approaches.
- We illustrated that using mainshock-only seismicity models leads to the hazard estimates that are biased low.
- Traditionally used hazard models should be critically assessed, and bias should be introduced with declustering adjusted.

Supplemental Material

INTRODUCTION

Traditionally, seismic hazard and risk assessment studies consider Poissonian occurrences of mainshocks, and disregard spatially and temporally dependent events (foreshocks and aftershocks), which are removed from earthquake catalogs before computing historical earthquake occurrence rates. The justification for this simplification is that the mainshock event (which is usually characterized as the event with the largest magnitude in a cluster) could, to some extent, represent the damage potential of the entire sequence. In the design world, this translates into implying that if the building is designed to withstand the ground-motion shaking of the mainshock, it will resist the assumed weaker ground motions of the other lower magnitude events in the sequence. However, several studies showed that this is an overly simplistic notion, because the different events in a sequence may have different epicentral areas, and the largest magnitude event does not imply the largest

1. University School for Advanced Studies IUSS Pavia, Pavia, Italy, https://orcid.org/0000-0001-5002-2222 (NŠ); https://orcid.org/0000-0001-6107-9451 (PB); 2. RED Risk Engineering + Development, Pavia, Italy, https://orcid.org/0000-0001-9151-0361 (MK); 3. Swiss Seismological Service, ETH Zurich, Switzerland, https://orcid.org/0000-0002-4546-8729 (ANP); 4. Università degli Studi di Napoli Federico II, Naples, Italy

*Corresponding author: nevena.sipcic@iusspavia.it

Cite this article as Šipčić, N., M. Kohrangi, A. N. Papadopoulos, W. Marzocchi, and P. Bazzurro (2022). The Effect of Seismic Sequences in Probabilistic Seismic Hazard Analysis, *Bull. Seismol. Soc. Am.* **XX**, 1–16, doi: 10.1785/0120210208

ground-motion intensity at any site. It is undeniable that earthquake sequences pose an additional risk to society because of the increment in financial losses due to increased direct damage to the built environment and to longer business interruption that follows. The underestimation of seismic risk by the traditional approach (here, by risk we refer to the ground-up losses to repair physical damage and not to insurance losses) is expected to be especially important in the period after the occurrence of a significant event due to the elevated short-term hazard (postmainshock conditions). This issue was extensively studied in past decades with the primary objectives of both supporting the decision-making process associated with emergency planning in the aftermath of an event and of helping communities prepare in periods of low seismicity for potentially destructive future earthquakes. These studies modeled the occurrence of subsequent events conditional on the occurrence of mainshock usually via the modified Omori law (Omori, 1894; Utsu, 1961) (e.g., Reasenberg and Jones, 1989; Wiemer, 2000; Yeo and Cornell, 2009; Gee *et al.*, 2021) or, more rarely, via the ETAS model (Ogata, 1988, 1998), such as in the studies of Field and Milner (2018) or Taroni *et al.* (2018).

Going beyond the postmainshock conditions, Boyd (2012) and Iervolino *et al.* (2014) extended the aftershock probabilistic seismic hazard analysis (APSHA) developed by Yeo and Cornell (2009). They identified independent clusters and combined probabilistic seismic hazard analysis (PSHA) and APSHA to calculate the annual exceedance rate of a ground-motion intensity level at a specific site due to all the events in clusters (sequence-based probabilistic seismic hazard analysis) rather than just to all the mainshocks. Along the same line, but using a different approach, Marzocchi and Taroni (2014) proposed a simple method based on the classical PSHA that introduced a correction for the negative bias (i.e., underestimation) caused by catalog declustering. For each cell in the domain, they suggested a correction to the total seismicity rate and the magnitude–frequency distribution (MFD) to make them equal to those computed from the whole (nondeclustered) catalog.

However, our objective is neither to perform the short-term forecast (i.e., to find the probabilities of exceeding ground-motion level conditional on the occurrence of the mainshock) nor to provide the seismic hazard estimates during the sequence. Similar to Papadopoulos *et al.* (2020), our goal is to include all the events in a sequence and not only the mainshock into the estimation of annual hazard but also, later, risk to specific structures and portfolios of them. To do so, we will generate sets of memory-full stochastic catalogs using as initial conditions the seismicity occurred until the time of the analysis. For this task, we will utilize the ETAS model, which is arguably state-of-the-art for modeling seismic sequences, both temporally and spatially.

Including all events in a sequence to calculate seismic rates is relevant, for example, to the insurance industry, where it is well known that traditional seismic risk assessment studies based on declustered catalogs underestimate the risk by neglecting sequences. To cover for such an unknown bias and other unknowns, insurance companies traditionally add significant loadings to the pure premium (i.e., the one based on the average annual loss) of earthquake insurance policies. Given that this bias is not well estimated, for business reasons this practice necessarily leads to an overcorrection of earthquake insurance premiums offered to the public. It is worthwhile noting, however, that exceptions to this practice exist, as some risk models make an attempt to somewhat consider seismic sequences. For instance, Shome and Williams (2014) included the occurrence of aftershocks while estimating the change in seismic risk in Japan, after the Tohoku earthquake, using the rates calculated with the Reasenberg and Jones (1989) methodology and averaging them over a five-year-long period.

As for the case of earthquake-resistant design, arguments in favor of using simplified approaches based on mainshock-only seismicity for risk assessment are not lacking. For example, the use of the mainshock-only approach in assessing seismic risk in the insurance industry is often supported by the logic that risk models are calibrated with the total damage (or claims) data collected at the end of sequences that include both damage (or loss) caused by mainshocks and damage (or loss) caused by aftershocks. This reasoning holds some truth when the time elapsed between the mainshock and the following events is short, and building inspection between events could not be done. This logic, however, is weak at the best for at least two reasons. First, in reality, risk models are only partially calibrated using damage or claims data. In many parts of the world, these data are simply not available, or no recent strong earthquakes have occurred in recent time, and the only data available may be for old events that affected a different building stock. Even when available, damage or loss data may come from sequences with mainshocks followed either by an intense activity or by hardly any activity. No difference between damage caused by one event or by a collection of events is considered during the calibration of the building vulnerability functions (i.e., relationships that link ground-motion intensity with repair cost) that are at the core of such earthquake risk models. The damage (or loss or claims) data, if available, are just used without further scrutiny. Second, in most cases, risk models are forced to use analytical studies to derive building vulnerability functions, at least, for the relatively recent building classes never tested by any severe earthquake. For these building classes, given the lack of empirical data and given that such analytical studies use only mainshock ground motions, the vulnerability functions are derived with a complete disregard of damage accumulation caused by multiple shocks. Even if the aftershock losses were perfectly embedded in the conventional vulnerability curves, which they are not, they would be applied to estimate the losses for the next event that may, or may not, be followed by an intense sequence. Therefore, it is abundantly clear that the current practice, strictly speaking, is far from being rigorous and should be improved. In this article, however, the focus

is on seismic hazard rather than risk, and, hence, these important considerations related to risk assessment in presence of clustered seismicity will be discussed in more detail in a future article.

To better understand the impact of sequences on seismic hazard estimates (which, in turn, affect risk estimates), we consider two cases. The first is the "unconditional case" (or "random year"), in which we sample multiple one-year-long stochastic catalogs, each one starting with different initial conditions. This exercise is meant to identify the average long-term increase in seismic hazard estimates due to sequences. This information could be helpful for applications that need stable hazard estimates that do not change whenever a significant event occurs (e.g., hazard maps informing building codes). The second is the "conditional case," which again considers multiple one-year-long stochastic catalogs; but, in this case, each one starts with the same initial conditions. This exercise is meant instead to identify the average long-term increase in seismic hazard estimates due to sequences at a particular point in time, information that is useful for applications such as pricing estimation for insurance policies to be issued in the period covered by the computation length (i.e., one year here).

Therefore, in the former case, the estimate of a hazard rate increase could have been computed by averaging the hazard estimates for simulated catalogs of any time length. We chose one year here, because usually hazard rates are presented for that time unit. In the latter case, however, we are interested in estimating the hazard at a specific time (perhaps after or during an intense sequence), conditional on the past seismicity in previous years. In this case, as alluded to above, the selection of the time length of the stochastic catalogs is clearly driven by the application. The time length of the simulated catalogs is the consequence of a practical decision rather than a conceptual one. Taking a one-year-long period is motivated by many real-world applications, particularly in the insurance industry, where earthquake risk estimates over one-year-long horizon starting at the time of the policy issuance are required, since earthquake policies are annual contracts. However, suppose an application calls for assessing the hazard increase over a longer period starting from the time of computation (e.g., three-year-long cat bonds). In that case, the proposed methodology can be replicated in an identical manner by simply lengthening the time of the simulated catalogs, as needed.

In the following sections, we first describe the ETAS model in relation to the simpler Omori law approach for modeling earthquake sequences and compare both with the Poissonian approach that, taken at face value, disregards them. Then, we investigate the variability of the estimates of the ETAS parameters in different regions of Italy and show that the ETAS model is capable of modeling realistic sequences with several tests. We then define the Poisson and Omori model, followed by the discussion about the effects of declustering on the Poisson model and the consistency of the Omori model with the available data. Finally, we estimate the hazard curves at the two selected sites with the three described methods, and we summarize our findings.

INITIAL CONSIDERATIONS ABOUT ETAS, OMORI, AND POISSON MODELS

Using a complex approach, such as ETAS, to model seismic sequences can be considered impractical, and this consideration motivated us to investigate two alternative, simpler models. The final considerations on the appropriateness of these three modeling choices that will follow are based on the comparison of seismic hazard curves for two sites in Central Italy computed in three ways: (1) using the ETAS model; (2) the classical mainshock-only Poissonian model; and (3) an approach that combines mainshock Poissonian modeling and aftershock modeling via modified Omori law (e.g., Iervolino *et al.*, 2014). We compare the hazard curves for the conditional and unconditional cases mentioned earlier in all the three modeling choices. To estimate the seismicity rate using the *b* and *c* models, it is necessary to agree on the (arbitrary) definition of what constitutes a mainshock. This definition guides the selection of the declustering method to adopt and, given the method adopted, of the specific values of the temporal and spatial parameters utilized for sifting out the foreshocks and aftershocks events in a cluster. Moreover, the parameter values of the modified Omori law to be used have to be coherent with the declustering technique adopted. It is well known that the selection of the declustering technique and its details can significantly affect the characteristics of the processed catalog and, therefore, the ensuing historical seismicity rates and, from there, the hazard results (Marzocchi and Taroni, 2014; Teng and Baker, 2019; Mizrahi *et al.*, 2021; Taroni and Akinci, 2021). Hence, as a part of this exercise, we examine some of the declustering methods available in the literature, namely Gardner and Knopoff (1974), Reasenberg (1985), Zaliapin *et al.* (2008).

However, for the correct utilization of the ETAS model, some considerations are in order. The ETAS model is calibrated based on the earthquake data available in the region of interest. Intuitively, we may assume that some ETAS parameters' values depend on the seismotectonic characteristics of the specific region. Several studies investigated the variability of the values of the ETAS parameters across different tectonic zones. For instance, Chu *et al.* (2011) explored the variability and fit of ETAS parameter values across different tectonic zones globally and identified significant differences. Similarly, Page *et al.* (2016) showed that aftershock productivity and decay rate vary with the tectonic regime. Utsu and Ogata (1995) found high variability of ETAS temporal parameter values and speculated that this variation might be related to the tectonic conditions of the region (such as structural heterogeneity, stress, or temperature). Nandan *et al.* (2017) applied ETAS in different regions of California and showed a significant spatial variation of the parameters' values. Conversely, Zhang *et al.* (2020) investigated the global

variability of ETAS parameters' values in subduction zones that experienced megathrust earthquakes with a magnitude larger than **M** 7.5 and showed no apparent systematic regional dependency. Stallone and Marzocchi (2019) also found no reason to assume a dissimilarity in the properties (in terms of productivity, duration, and spatial distribution) of clusters occurring in different active crustal regions.

It remains unclear whether it is justified to use the same set of ETAS parameters' values in a large area, such as a continent or a country. Ideally, one could distinctly consider regions with different seismotectonic characteristics and estimate parameters' values specific for each region. However, there are often practical complications in doing so. For example, scarcity of data sometimes poses difficulties in obtaining robust estimates in each region. Even when enough data are available, a somewhat complicated mathematical framework is required to properly treat the parameter variation around the boundaries of the two regions, given that events in one region could trigger events in the adjacent one and vice versa. To address these practical issues, we explore the variability of the estimates of ETAS parameters in two different regions in Italy fitted using a common instrumental catalog.

BUILDING THE ETAS MODEL

To familiarize the reader with the ETAS model, we first review its fundamentals defined by Ogata (1988, 1998). The ETAS model is one of the space–time point Hawkes processes formulated as the combination of background seismicity and triggered seismicity. Every background (or parent) event can trigger offspring events potentially capable of producing offspring of their own. Thus, the overall rate of events (sometimes called conditional intensity) with magnitude m at a certain point in time and space, conditional upon the history of prior earthquakes H_t can be characterized by the general form given with the following equation (Zhuang *et al.*, 2004; Seif *et al.*, 2017):

$$\lambda(t,x,y,m|H_t) = \mu(x,y) + \sum_{j:t_j<t} g(t-t_j, x-x_j, y-y_j; m_j). \quad (1)$$

The index j refers to all past earthquakes. For simplicity and computational benefit, we assume that the background rate is stationary in time, that is, $\mu(t,x,y) = \mu(x,y)$, even though this assumption may not always be valid (Lombardi and Marzocchi, 2007). A triggering function$g(t-t_j, x-x_j, y-y_j; m_j)$, which comprises a productivity function, a temporal distribution, and a spatial distribution, gives the rate of triggered events. The function g has the following form (Ogata, 1998):

$$g(t-t_j, x-x_j, y-y_j; m_j) = Ae^{\alpha(m_j-m_c)}(p-1)\times c^{p-1} \times (t-t_j+c)^{-p} f(x-x_j, y-y_j, m_j). \quad (2)$$

The productivity term $k(m_j) = Ae^{\alpha(m_j-m_c)}$ represents the mean number of events directly triggered by an earthquake of a magnitude m_j, in which m_c is the minimum magnitude considered. The temporal decay of triggered earthquakes, namely $v(t-t_j) = (p-1)\times c^{p-1}\times(t-t_j+c)^{-p}$, is modeled with the so-called Modified Omori law (Omori, 1894; Utsu, 1961). Although productivity and temporal distribution adopted by researchers are typically the same, spatial distribution $f(x-x_j, y-y_j, m_j)$ can be found in several formats. The one adopted in our study showed good performance in Papadopoulos *et al.* (2020) and Zhuang *et al.* (2004):

$$f(x-x_j, y-y_j, m_j) = \frac{q-1}{\pi \times d \times e^{\gamma\times(m_j-m_c)}}\left[1+\frac{(x^2+y^2)}{d\times e^{\gamma\times(m_j-m_c)}}\right]^{-q}. \quad (3)$$

It is worthy that the adopted spatial distribution uses a simple isotropic kernel. This means that the spatial distribution has no knowledge of the location of existing faults in the region, and it does not eliminate the possibility that an aftershock is triggered exactly at the same location of the mainshock, which is a rather unrealistic case. Ogata and Zhuang (2006) corrected this deficiency using an anisotropic kernel instead, but they showed that the model's performance does not change significantly. More recently, Fitzenz and Langenbruch (2021) showed that using magnitude-dependent kernel weights can improve earthquake forecast performance (seen using the log-likelihood score) for large events. However, given its heavy computational burden, these enhancements are not considered here.

The magnitude distribution $s(m)$ of both background and triggered events, which is assumed to be independent of the other terms, follows the exponential Gutenberg–Richter law, truncated at maximum magnitude m_{max}. Other models for $s(m)$ can also be used (e.g., tapered Gutenberg–Richter):

$$s(m) = \frac{\beta e^{-\beta(m-m_c)}}{1-e^{-\beta(m_{max}-m_c)}}. \quad (4)$$

The constant β is equal to $\ln(10)b$, in which b is estimated independently from other parameters using the maximum-likelihood method (Aki, 1965) and accounting for the magnitude binning correction (Utsu, 1966). One should keep in mind that the method of Aki (1965) was developed for nontruncated magnitude distribution, and, hence, the b-value estimate in equation (4) might be biased. Marzocchi *et al.* (2020) showed, however, that the bias is not significant when$M_{max} - M_{min} \geq 3$.

As in all empirically based exercises, to obtain reliable estimates of the ETAS parameters' values (A, α, p, c d, γ, and q), it is necessary to have a complete and homogenous catalog with a "sufficient" amount of data. The catalog should: (1) extend beyond the considered region to prevent estimating an artificially lower density near the geographical boundaries by

excluding offspring inside the border generated by earthquakes in the outer region (Wang, Jackson, and Zhuang, 2010); and (2) extend beyond a temporal window before the starting time T_0 of the investigation period to include events within the investigation period that may be triggered by earthquakes that occurred before T_0. For these reasons, we extend the studied region for 75 km outside of the borders and include two years of seismicity as initial conditions before the beginning of the investigation period T_0.

In our application, the estimates of the values of the ETAS parameters are found by maximizing the log-likelihood function expressed with

$$\log L(\theta) = \sum_{j=1}^{n} \log[\lambda(t_j, x_j, y_j|H_t)] - \iint_0^{S,T} \lambda(t, x, y|H_t) dtds, \tag{5}$$

in which S and T are the spatial and temporal windows, respectively, whereas n represents the number of events in them (Seif *et al.*, 2017). The background seismicity rate $\mu(x, y)$ can be written as $\nu \times u(x, y)$, in which ν is the total rate, and $u(x, y)$ is the spatial distribution of the background events. To simplify the maximization procedure, the spatial distribution $u(x, y)$ of the background seismicity rate is computed separately from all the other parameters using first the mainshock-only catalog (obtained using the original Gardner and Knopoff, 1974 declustering algorithm) and then smoothing the mainshock rate using the Gaussian kernel-based smoothing approach proposed by Frankel (1995) with a correlation distance of 20 km. For an interested reader, the effect of different background models and different correlation distances can be found in Papadopoulos *et al.* (2020). The value of ν is estimated together with the rest of the ETAS parameters.

The value of the productivity parameter α controls the triggering capability of events with respect to the magnitude. A high value of α implies that a higher triggering capability is given to the events with higher magnitudes, whereas low value gives more capability to lower magnitude events. Several studies showed that the value of α is found to be lower than $\beta = \ln(10)b$ (Console *et al.*, 2003; Ogata and Zhuang, 2006; Chu *et al.*, 2011). However, other researchers claimed that this trend is observed due to the unrealistic assumptions of the model (such as isotropic kernel for aftershock distribution) and that, in reality, $\alpha \cong \beta$ an alternative that agrees with the Båth's law (Felzer *et al.*, 2003) and stress-triggering models (Hainzl *et al.*, 2010). Furthermore, Hainzl *et al.* (2013) found that when the aftershock incompleteness and time variance of the background rate are accounted for, results imply that $\alpha \cong \beta$. Although the debate about the appropriate α-value remains open in the scientific community, we adopt here $\alpha = \beta$ and consider a vector of unknown parameters as

$$\theta = \{\nu, A, c, p, d, q, \gamma\}. \tag{6}$$

A more comprehensive overview of the ETAS model can be found in Ogata and Zhuang (2006).

SEISMICITY DATA

Several studies showed that the estimates of the ETAS parameters are highly susceptible to the assumptions made, such as magnitude cutoff, time dependency of the background rate, anisotropic aftershock triggering, and aftershock incompleteness (Seif *et al.*, 2017; Zhuang *et al.*, 2017). Keeping the earlier in mind, it is evident that it is not straightforward to compare parameters' values from different studies that use different catalogs (with varying quality, magnitude of completeness, and spatial and temporal windows). In addition, the underlying statistical correlation of the parameters is complicating the comparison even further. Detecting the source of the potential differences between parameters' values can become very challenging, as different sets of values can lead to very close values of the log-likelihood functions (Lombardi, 2017).

The first objective of our study is to compare the discrepancies of the parameters' values across two different regions in Italy. To make the comparison more straightforward and consistent, we use the same earthquake catalog, identical temporal windows, and the same minimum magnitude of completeness. The spatial extent of the defined regions is shown in Figure 1. Region 1 is associated with the part of Italy where significant sequences were observed in the recent past, whereas region 2 is an area of high seismicity but with less observed activity in the recent past. The data used in this study are obtained from the instrumental earthquake catalog of Lolli *et al.* (2020) (HOmogenized instRUmental Seismic [HORUS] catalog, see Data and Resources), homogenized to the moment magnitude M_w within a polygon that covers the mainland of Italy. We select the time window between 1983 and 2020 as the investigation period, with the previous two years (1981–1983) as the auxiliary window. In the considered investigation period, five events with $M_w \geq 6$ with a maximum magnitude of M_w 6.6 occurred in region 1, whereas all events have $M_w < 6$ in region 2. The data are restricted to events with a maximum hypocenter depth of 40 km. Using this dataset, we estimate the Gutenberg–Richter law's b-value as 1.03 and 1.04 for regions 1 and 2, respectively. In addition, the minimum completeness magnitude M_w 3 of this catalog is estimated as the value at which the hypothesis of exponentially distributed data cannot be rejected at a significance level of 0.05 (Lilliefors, 1969). The same dataset is used later in this study for underpinning the Poisson and Omori models.

REGIONAL DEPENDENCY AND COMPARISON OF ETAS MODEL WITH HISTORICAL SEISMICITY

Using the model described in the previous sections and the HORUS instrumental catalog, we find the maximum-likelihood estimates (Table 1) of the ETAS parameters for the two considered regions. To test the robustness of these

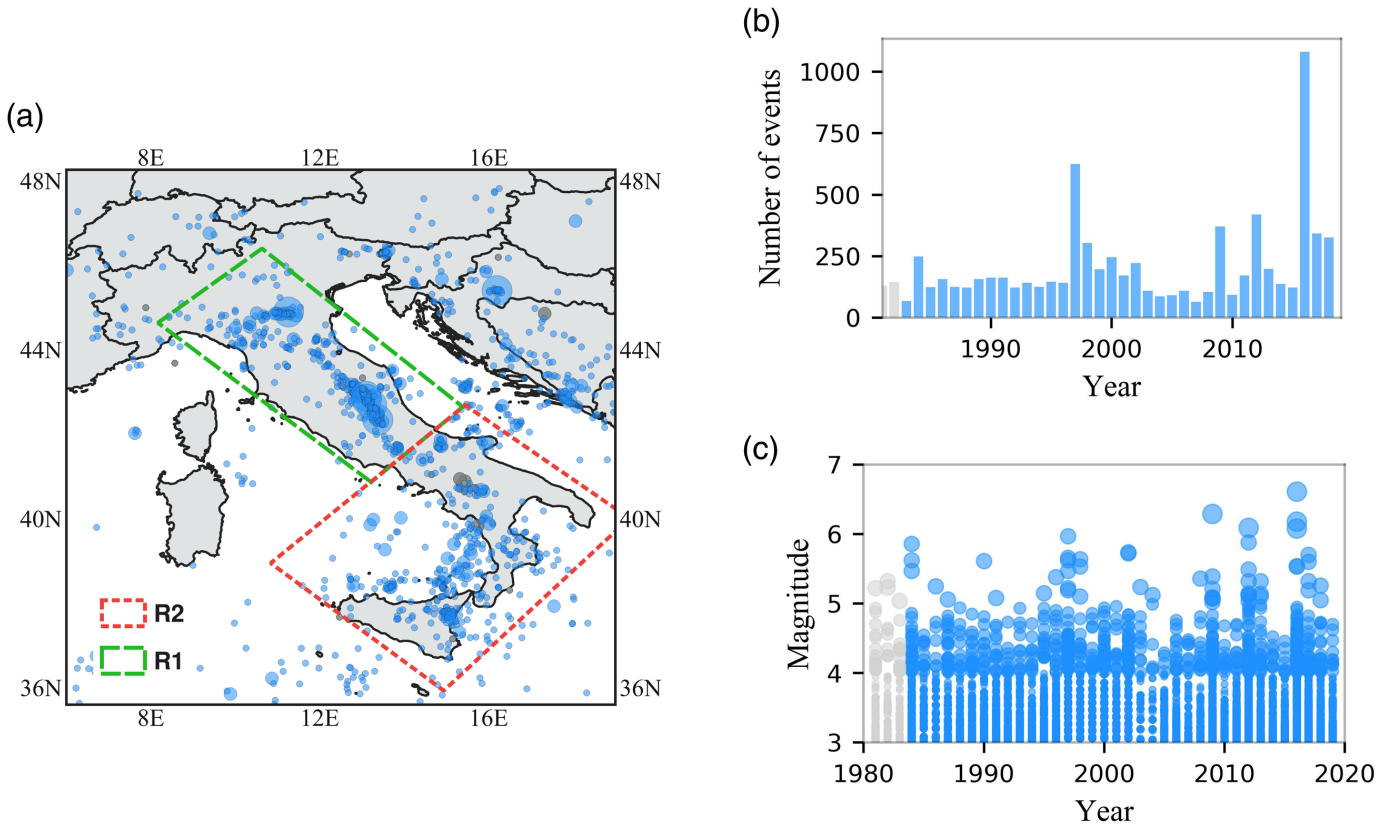

Figure 1. (a) Spatial extent of the considered regions. Dots represent the earthquakes' epicenters, and their size is proportional to the magnitude; (b) the number of earthquakes per year; and (c) temporal distribution of the events shown in (a). In all the figures, blue is used for events in the target temporal window (1983–2020) and gray for events in the auxiliary temporal window (1981–1983). The color version of this figure is available only in the electronic edition.

estimates, we use different lengths of the auxiliary windows (from 2 to 10 yr) and observe minor differences in estimates (see the supplemental material available to this article for details). Furthermore, we estimate the standard errors of the parameters following the procedure of Wang, Schoenberg, and Jackson (2010), simulating 200 stochastic catalogs and using the values given in Table 1. The standard error of each parameter's estimate is given in the brackets. In addition, we show the total background rate calculated by integrating the spatial distribution $u(x, y)$ over the target region and multiplying it by the estimated value of the total rate ν. Finally, we estimate the branching ratio, representing the proportion of the triggered events amongst all events, to get a better insight into the triggering properties. The branching ratio, for the case when $\alpha = \beta$, is estimated as (Zhuang *et al.*, 2013) follows:

$$n = \int_{m_c}^{m_{max}} k(m)s(m)dm = \frac{A \cdot \beta(m_{max} - m_c)}{1 - e^{-\beta(m_{max}-m_c)}}. \quad (7)$$

TABLE 1
Estimated Mean Values and Standard Errors (within Brackets) of the Epidemic-Type Aftershock Sequence (ETAS) Parameters

ETAS Parameter Estimates	Region 1	Region 2
$\hat{\nu}$	0.92 (0.11)	0.945 (0.088)
$\hat{A}$ (events/day/km^2)	0.093 (0.014)	0.09 (0.044)
$\hat{c}$ (days)	0.02 (0.004)	0.0054 (0.0029)
$\hat{p}$	1.18 (0.02)	1.08 (0.044)
$\hat{d}$ (km^2)	0.9 (0.15)	1.66 (0.28)
$\hat{q}$	2 (0.17)	1.81 (0.16)
$\hat{\gamma}$ (magnitude^{-1})	0.59 (0.12)	0.36 (0.14)
Number of events	4323	2835
Total background rate (events/day)	0.076	0.106
Branching ratio	0.96	0.92

There are some evident differences in these sets. For instance, the branching ratio in region 1 is higher, which was expected, given that significant sequences were observed in this region since 1983. Furthermore, based on the temporal parameters p and c, one can find that 50% of the triggered events are expected to occur within one day in region 1, whereas 32 days are needed in region 2. It is difficult to establish with certainty the origin of these differences, as it could be attributed to the parameter bias, model deficiency, actual differences in the properties of the earthquake phenomenon, or a combination of the above.

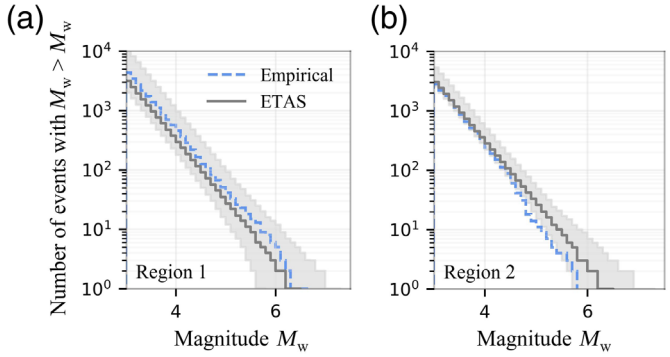

Figure 2. Magnitude–frequency distribution (MFD) of the events in the observed and stochastic catalogs for the period of 1983–2020 in (a) region 1 and (b) region 2. The blue dashed line refers to the instrumental HOmogenized instRUmental Seismic (HORUS) catalog, the solid gray line is the median of 500 epidemic-type aftershock sequence (ETAS)-generated catalogs, and the shaded area represents the 5th and 95th percentiles of the ETAS simulations. The color version of this figure is available only in the electronic edition.

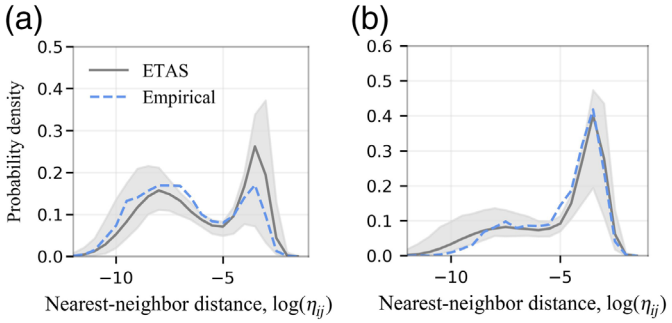

Figure 3. Distribution of the nearest-neighbor distance η_{ij} for the period of 1983–2020 for (a) region 1 and (b) region 2. The solid gray line refers to the median of 500 ETAS generated catalogs; the dashed blue one to the instrumental catalog and the shaded area represents 5th and 95th percentiles of the ETAS-generated catalogs. Histograms are illustrated with continuous lines rather than bars for clarity. The color version of this figure is available only in the electronic edition.

That said, we perform several Turing-style tests (Page and van der Elst, 2018) to verify that the ETAS-generated synthetic catalogs can be considered a realistic representation of the physical phenomenon (i.e., if they are statistically consistent with the observed seismicity). To this end, we generate 500 stochastic catalogs describing the seismicity from 1983 to 2020, conditioned on the history of the two previous years (1981–1983), and compare their characteristics with those of the observed data. If the ETAS-based catalogs are significantly different from the observed data, one could conclude that the model cannot reproduce the characteristics of the observed seismicity. In this section, we show only two of these tests for conciseness. Additional tests can be found in the supplemental material. These tests are by no means exhaustive but are nonetheless indicative of the robustness of the approach.

First, we compare in Figure 2 the cumulative MFD of observed and ETAS-simulated events in the 37 yr long observation period. The observed number of earthquakes lies within the 5th and 95th percentiles extracted from the simulated catalogs, for region 1, whereas some discrepancy is observed for region 2.

In addition, we compare the ETAS model's clustering behavior with that of the observed seismicity adopting the analysis of Zaliapin *et al.* (2008). Identifying clusters with this method is centered on estimating the proxy inversely proportional to the strength of the "bond" between the two earthquake events. This proxy represents the nearest-neighbor distance in a multidimensional domain (time, location, and magnitude), and it separates the space into two subdomains: one (with lower η_{ij}) likely contains clustered events, and the other (with higher η_{ij}) likely contains background events. Nearest-neighbor distance can be found as per equation (8), in which t_{ij} is the temporal distance, r_{ij} is the spatial distance between events i and j, and d is a constant taken equal to 1.3 following (Peresan and Gentili 2020):

$$\eta_{ij} = \begin{cases} \tau_{ij} r_{ij}^{d} 10^{-bm_i}, & t_{ij} > 0 \\ \infty, & t_{ij} \le 0 \end{cases}. \tag{8}$$

Again, stochastic catalogs are used to find the η_{ij} distribution. Figure 3 compares the median and the 5th and 95th percentiles of ETAS-simulated catalogs with the observed seismicity for both regions. The separation between the background and clustered modes is clear in region 1, whereas the background peak dominates the distribution in region 2. We can see that in region 1 the ETAS-based median of the clustered mode is overestimated and that of the background slightly underestimated. However, in general, the characteristics of simulated and observed catalogs show a good match.

Even though we can see nonnegligible differences in the clustering properties between these regions, we argue that this is a matter of the limited amount of sequences in southern Italy rather than due to intrinsic dissimilarities in the earthquake phenomena. In fact, only very few rich sequences were observed in this period outside of Central Italy. To test the validity of this assumption, we use the CPTI15 catalog (Rovida *et al.*, 2020) (see Data and Resources) to get more information regarding the high-magnitude events that are not plentiful in the HORUS catalog. This catalog, assembled as a combination of harmonized macroseismic and instrumental Italian data, covers the period from 1000 to 2017, and it is considered complete for events of **M** 6 and above.

We simulate 100 stochastic catalogs of events spanning from 1717 to 2017 in region 1 using the parameters calibrated based on the HORUS catalog and region 1. Then, we repeat the exercise for region 2 but using two sets of parameters' values: the set of parameters calibrated for region 2 (second column in Table 1) and the set of parameters calibrated for region 1 (first column in Table 1). The **M** 6+ events of all simulated catalogs are then compared with the **M** 6+ events included in the CPTI15 catalog.

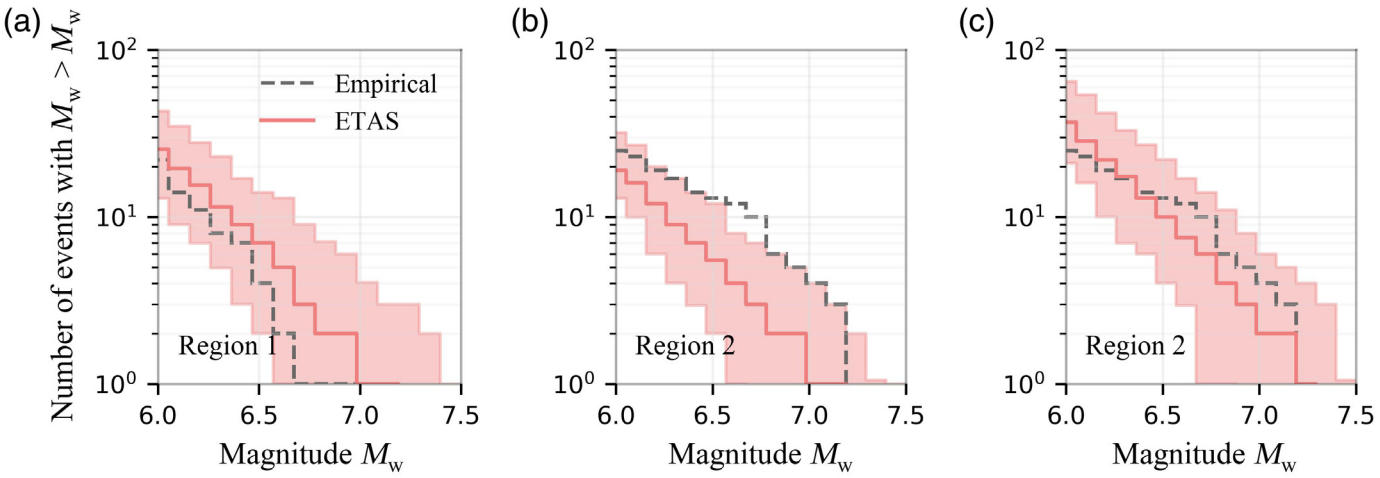

Figure 4. MFD of the observed and stochastic catalogs for the period of 1717–2017 in (a) region 1, using parameters of region 1, (b) region 2, using parameters of region 2, and (c) region 2, using the parameters of region 1. The gray dashed line refers to the historical CPTI15 catalog, the red line is the median and the shaded area is 5th and 95th percentiles of the 100 ETAS-generated catalogs. The color version of this figure is available only in the electronic edition.

First, it is essential to acknowledge that in region 1 ETAS can predict the historical seismicity well, even though the model is calibrated using a different catalog (see Fig. 4a). There is some overestimation of results, possibly because the last 40 yr for which the parameters are calibrated, were particularly active, but not significantly. Second, in region 2, one can observe that the set of parameters from region 1 provides MFD closer to the observed one (see Fig. 4b,c). Based on these results, we speculate that using the set of parameters from region 1 where the observed seismic sequences are plentiful and, therefore, the parameters' values are well-constrained yields more defensible seismicity estimates in region 2.

It is worth noting that assuming that the ETAS parameters in these regions are the same does not mean that the total background rates are equal. More specifically, we assume that the ratio between background events (computed within the maximization procedure) and the events in the declustered catalog we used is the same for the three regions. However, this assumption does not imply that the total background rate is the same.

POISSON AND OMORI MODELS

To use the model that combines Poisson and Modified Omori law, it is necessary first to simulate Poissonian mainshock events. To do so, we decluster the catalog, then calculate MFDs and rates using a correlation distance of 20 km, which is also used for the background seismicity in ETAS. For every mainshock event, we generate aftershocks following the Reasenberg and Jones (1989) methodology. Within this formulation, the rate of aftershocks with magnitude $\geq m_c$ at time t (time elapsed since the mainshock event) is found using the combination of the temporal (Omori, 1894) and productivity (Utsu, 1961) laws as

$$\lambda(t, m_c) = 10^{a+b(m_j-m_c)}(t+c)^{-p}, \tag{9}$$

in which a, c, and p are the model parameters, whereas b is the value from the Gutenberg–Richter law. To estimate the parameters' values, we maximize the log-likelihood function, given by

$$\ln L(a, c, p) = \sum_{i=1}^{N} \ln \lambda(t_i) - \int_{t_0}^{t_{\text{end}}} \lambda(t)dt, \tag{10}$$

in which N is the number of aftershocks, whereas t_0 and t_{end} refer to the beginning and the end of the period considered, respectively. Reasenberg and Jones (1989) proposed probability distributions for these parameters, fitting several California sequences, later extensively used in seismic forecasting. Estimating the Omori parameters with sequence-specific fits can be challenging, as many sequences do not have aftershocks above completeness magnitude, whereas simply disregarding these sequences causes a positive bias in the estimate of the productivity parameter a. That said, it is now well recognized that Reasenberg and Jones (1989) overestimated the value of a, as they only considered sequences with a sufficient amount of aftershocks (Felzer *et al.*, 2003). In our study, we use instead the methodology proposed by Page *et al.* (2016), utilized as a foundation for short-term aftershock forecasting at the U.S. Geological Survey, for which, to get better-constrained results, all sequences relative to the corresponding mainshock's time are stacked together, and mean Omori parameters are estimated. Based on the sequences identified with the chosen methodology (which we discuss in the following sections), the equivalent earthquake magnitude is estimated as $(\frac{1}{b}) \log_{10} \sum_{j=1}^{K} 10^{bM_j}$, in which K is the number of mainshocks in the stack (Hardebeck *et al.*, 2019).

As the proposed model is purely temporal, to model aftershocks' spatial distribution, we use a simple circular area around the mainshock with a radius equal to three rupture lengths estimated with the (Wells and Coppersmith, 1994)

scaling law. Although we are aware that this model might be overly simplistic, a detailed investigation of the aftershocks' spatial distribution is outside the scope of our work.

The approach described earlier is extensively used in the literature to model earthquake sequences, because it has the advantage of having fewer parameters to estimate than ETAS, and it builds on the familiar mainshock-only Poissonian model and upgrades it. We believe, however, that this approach has some critical weaknesses, which we address in the following subsection.

Effect of declustering on Poisson model

The Poissonian rates of occurrence of mainshocks are empirically estimated from declustered catalogs, which are obtained using declustering techniques. These techniques, however, are plagued by several arbitrary decisions that inevitably color the final results. To investigate the declustering caveats, we apply here three different techniques to the HORUS catalog for region 1, minimum magnitude **M** 3, and the period from 1981 to 2020.

The most used and the simplest declustering technique is the window-based Gardner and Knopoff (1974; hereafter, GK74) method. The algorithm identifies the largest **M** event in a sequence, and removes all other events within a window with **M**-specific prespecified temporal and spatial parameters centered at the identified event. A more complex declustering approach was later proposed by Reasenberg (1985; hereafter, R85), who extended the work of Savage (1972). Their idea was to link every event to a cluster via a spatiotemporal proxy. Every event linked with the prior one joins its cluster and, therefore, clusters grow by association. In this manner, the spatiotemporal window does not solely depend on the mainshock magnitude (as it does in GK74) but instead varies with events' behavior. More precisely, the spatial extension is based on the stress distribution pattern, which is assumed to depend on the cluster's last and the largest event. The temporal extension is developed based on the probabilistic model and Omori law. More details about the model can be found in Reasenberg (1985), Molchan and Dmitrieva (1992), van Stiphout *et al.* (2012). Finally, we use the nearest-neighbor proxy defined by Zaliapin *et al.* (2008; hereafter, ZNN) to identify the sequences, the largest event of which is kept as the mainshock. More details about this model are given in the previous section. One should bear in mind that the declustering methods mentioned earlier might be affected by the parameters that define them, calibrated based on a particular region and limited amount of data. They may or may not be the optimal set of parameters for other regions but are nonetheless used extensively in the literature. Besides the GK74, R85, and ZNN considered here, several other methods for identifying sequences can be found in the literature, from simple deterministic ones to more advanced stochastic ones such as Zhuang *et al.* (2004), Zaliapin and Ben-Zion (2020), or Llenos and Michael (2020). This high number of available declustering methods clearly reflects the true difficulties in reliably classifying earthquake events.

TABLE 2
Properties of the Declustered Catalogs (Region 1, M_{min} = 3, Period 1981–2020)

Method	GK74	R85	ZNN
MS	1191	2240	1151
AS	2513	1857	2610
Ratio*	26.8	50	25.9
p-value (M_{min} = 3)	3.7×10^{-2}	10^{-18}	3×10^{-4}
p-value (M_{min} = 3.5)	4×10^{-2}	1×10^{-5}	42×10^{-2}

AS, aftershock; GK74, Gardner and Knopoff (1974); MS, mainshock; R85, Reasenberg (1985); ZNN, Zaliapin *et al.* (2008).
*Full to declustered catalog.

As stated earlier, one of the main objectives of declustering is to obtain a catalog of earthquakes (mainshocks) for which the temporal occurrences can be modeled as a Poissonian distribution. A check of whether the Poissonian process assumption holds is rarely carried out in practice. As Luen and Stark (2012) showed, whether the declustered catalog could be considered Poissonian depends on the declustering method, available catalog, magnitude range, and the statistical test utilized. Therefore, we first test the Poissonian assumption with the Kolmogorov–Smirnov one-sample test following Luen and Stark (2012), and we show its p-values in Table 2. The p-values obtained for all three declustered catalogs are low (below 5%), with the GK74 catalogs yielding the highest values and the R85 ones yielding the lowest. This trend, also observed in other studies, led to the use of GK74 for declustering the catalogs adopted in National Seismic Hazard Models (NSHMs), for example, MPS19 for Italy (Meletti *et al.*, 2021) and NSHM for the United States (Petersen *et al.*, 2020). Table 2 also compares the number of events in the entire catalog with the number of events in the three declustered catalogs. From these results, one can see that the R85 method retains by far the highest number of mainshocks, whereas GK74 and ZNN yield similar results.

On a different note, keeping only the largest events in the clusters might affect the b-value due to the Gutenberg–Richter law's inevitable distortion. The declustering technique removes a disproportionately much larger number of lower magnitude events than higher magnitude ones (i.e., it does not sample the Gutenberg–Richter distribution randomly), and, therefore, it tends to lower the estimate of the b-value. To check that the magnitude of the events in the three declustered catalogs can still be reasonably modeled with an exponential distribution, we use the Lilliefors (1969) test and conclude that the hypothesis of exponential distribution cannot be rejected at a significance level of 5% in all the three cases. Figure 5 shows the Gutenberg–Richter distribution (hereafter referred as GR) and associated b-values for the three declustered catalogs to illustrate that significantly lower values were obtained for GK74 and ZNN models. On the contrary, the catalog declustered with R85 has the same b-value as the full catalog. The issue

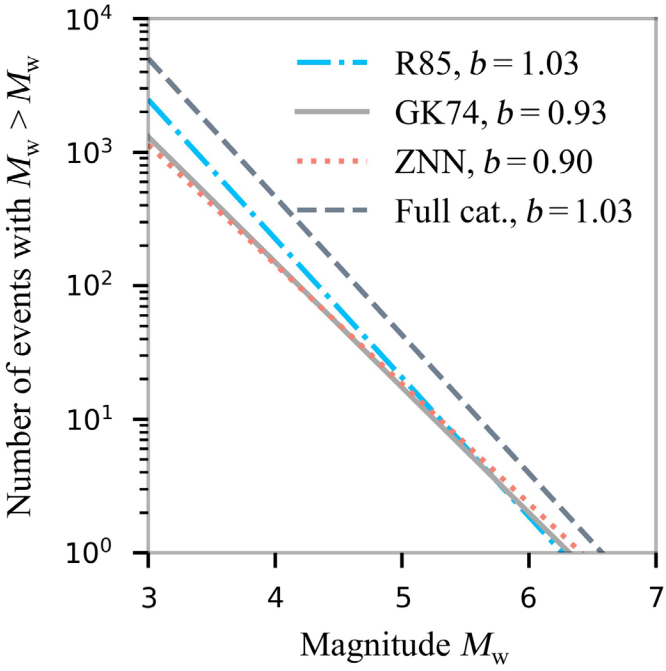

Figure 5. Gutenberg–Richter law for the full HORUS catalog and for three different declustered catalogs extracted from it (figure refers to region 1). The color version of this figure is available only in the electronic edition.

related to the distortion of the GR *b*-value due to declustering was acknowledged in the Uniform Californian Earthquake Rupture Forecast version 3 (Field *et al.*, 2014), in which, for the MFD of the gridded seismicity model, the *b*-value of the declustered catalog was used only before the point where MFDs of the full and declustered catalogs crossover. Nonetheless, a common practice in PSHA is still to take the *b*-value of the declustered catalog as is and, therefore, to overestimate the rate of high-magnitude events in hazard calculations possibly considerably (Mizrahi *et al.*, 2021).

Finally, one should note that the declustering also affects the spatial distribution of the events, as recently illustrated by Llenos and Michael (2020). Spatial distribution of events declustered with the three different methods can be found in the supplemental material.

Keeping the earlier discussion in mind, one needs to be careful with the interpretation of the declustering results, because it is not guaranteed that the occurrence of the remaining events can be reasonably modeled with a Poisson distribution. In addition, it is necessary to be aware of the sensitivity to the chosen method, as different catalogs declustered from the same initial catalog can have significantly different numbers of events and different *b*-values of Gutenberg–Richer law.

Consistency of the Omori model with the available data

Using the three models previously described (GK74, R85, and ZNN) and the methodology presented in the previous section, we estimate the values of the Omori parameters for region 1, minimum magnitude **M** 3, and the period 1981–2020. It is essential to highlight that the values of the set of Omori parameters obtained here differ from the values of the set estimated in the ETAS model (first column of Table 1), because the values of the Omori parameters in ETAS are applied locally, that is, to every generation of aftershocks. In the modified Omori law model, on the other hand, all aftershocks are assumed to be triggered by a single mainshock event, and, hence, the parameters' values refer to entire sequences. Therefore, the applicability of the modified Omori–Utsu law is questionable in cases with complex sequences as frequent occurrence of large aftershocks, which might trigger their own sequences, can break the Omori law assumed for the entire sequence (Spassiani and Marzocchi, 2018). Furthermore, several studies showed that aftershock productivity could significantly vary from sequence to sequence, suggesting that differences in the tectonic region (Chu *et al.*, 2011; Page *et al.*, 2016), geometry of source (Dascher-Cousineau *et al.*, 2020), mainshock stress-drop variability (Marsan and Helmstetter, 2017), and heat flow (Zaliapin and Ben-Zion, 2016) might be potential reasons. Hence, assuming the same value of the productivity parameter (*a* in Omori and *A* in ETAS) for all sequences can cause bias, reducing the sequence-to-sequence variability. Even though this problem is mutual for both the ETAS and Omori models, ETAS benefits from some natural variability intrinsic in the model.

The derived parameter estimates are presented in Figure 6. To better assess the reasonability of the Omori law parameter values obtained from the GK74, R85, and ZNN declustering methods, we generate 500 stochastic catalogs in region 1 over the 1983–2020 period (previous two years of seismicity are used to feed the model, similarly as in the ETAS case) using Monte Carlo simulation. In this exercise, we estimate the number, magnitude, location, and time of the aftershocks generated by each mainshock event simulated via the Poisson model and compare them with the observed values in the HORUS catalog. The *b*-value for simulating the mainshocks is given in Figure 5, whereas we use 1.03 (*b*-value of the full catalog) for the aftershocks, as this is a common approach in the literature. In addition, the magnitudes of the generated aftershocks are constrained to be lower than the corresponding mainshock's magnitude for consistency with the assumption adopted in the three declustering techniques. Figure 7a compares the MFD of the earthquakes in the 500 simulated catalogs with the one of the HORUS catalog. In all cases, the match is satisfactory, even though the parameters used are somewhat different.

As we use different *b*-values for simulating mainshocks and aftershocks in the Omori model, the *b*-value of the resulting simulated catalog remains unclear. That said, we estimate the median and 90% confidence interval based on the 500 Omori simulated catalogs, and compare them with those of the 500 ETAS-simulated catalogs and with the original *b*-value of the HORUS full catalog (Fig. 7b). With all Omori variants, the

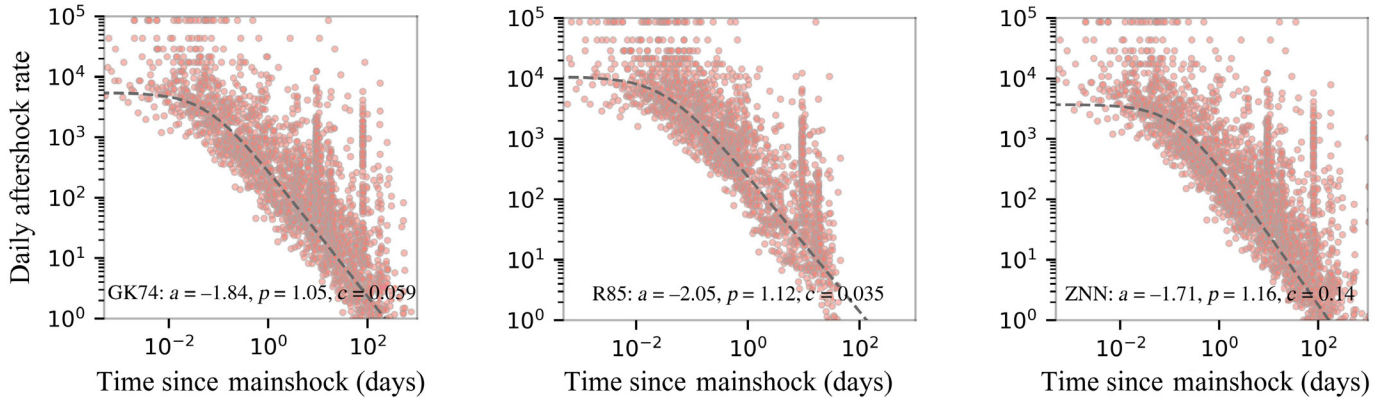

Figure 6. The stacked rate of aftershocks following mainshocks from 1981 to 2020 in region 1 (the minimum magnitude considered for both mainshock and aftershock events is **M** 3). The gray solid line shows the aftershock rate obtained with the Reasenberg and Jones (1989) model, whereas the empirical aftershock rate was found from two consecutive aftershocks in the stack as $1/(t_{i+1} - t_i)$ (Hardebeck *et al.*, 2019). From left to right, the method used to identify sequences is Gardner and Knopoff (1974, referred as GK74), Reasenberg (1985, referred as R85), and Zaliapin *et al.* (2008, referred as ZNN), respectively. The color version of this figure is available only in the electronic edition.

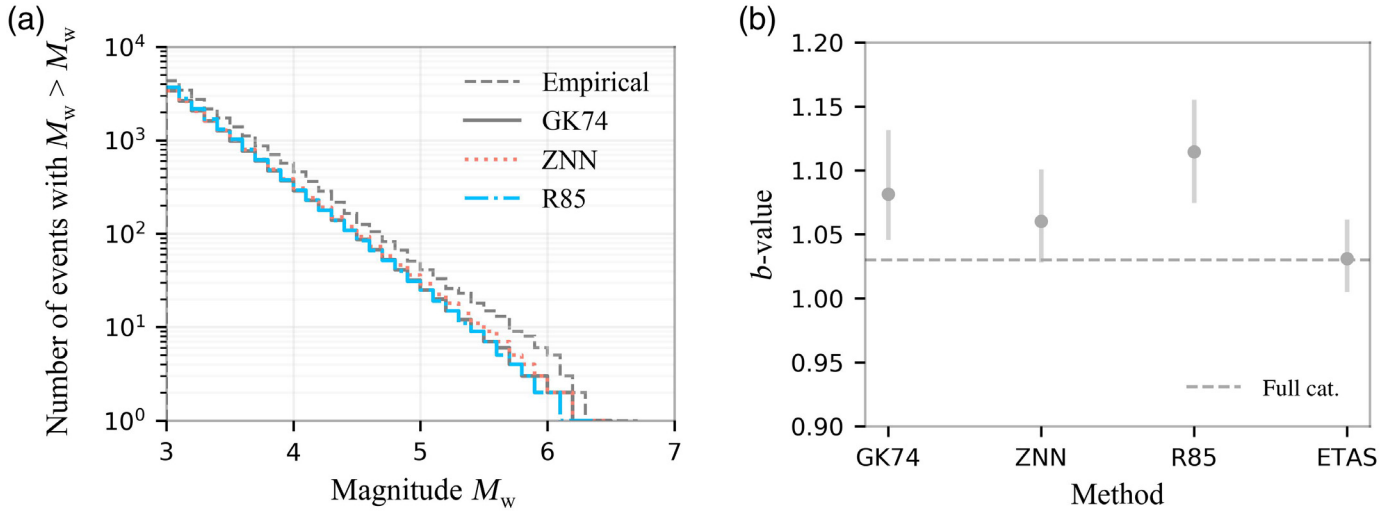

Figure 7. (a) MFD of the observed and simulated catalogs for the 1983–2020 period in region 1. The dashed gray line refers to the instrumental HORUS catalog, whereas other lines refer to the median of 500 Omori-generated catalogs using different sets of parameters' values; (b) Median and the confidence intervals for *b*-value estimated based on the 500 simulations, for different models. The color version of this figure is available only in the electronic edition.

b-value of the simulated catalogs is higher than the original, whereas this value is perfectly recovered in the case of ETAS. To the authors' knowledge, this issue with the Omori model is not recognized in the literature, and the *b*-value of the resulting stochastic events, which is somewhat arbitrary, is left unchecked.

HAZARD ESTIMATES

In this section, we compare and contrast the hazard estimates in terms of SA (0.3 s) (spectral acceleration at the period of 0.3 s), at two rock sites (shear-wave velocity in the top 30 m of 800 m/s) in Norcia and Perugia (region 1, central Italy), obtained from different catalogs that use the Poisson, Poisson + Omori, and ETAS approaches to model earthquake occurrences. More specifically, we simulate 20,000 one-year-long stochastic catalogs of seismicity in region 1 using these three approaches. To each event in the catalog, rupture properties, such as a rake, dip, slip, and seismogenic depth, are generated using the Seismic Harmonization in Europe seismic source model (Woessner *et al.*, 2005), following the procedures implemented in the OpenQuake software (Pagani *et al.*, 2014). We used the (Abrahamson *et al.*, 2014) ground-motion prediction equation to characterize the ground motion generated by each

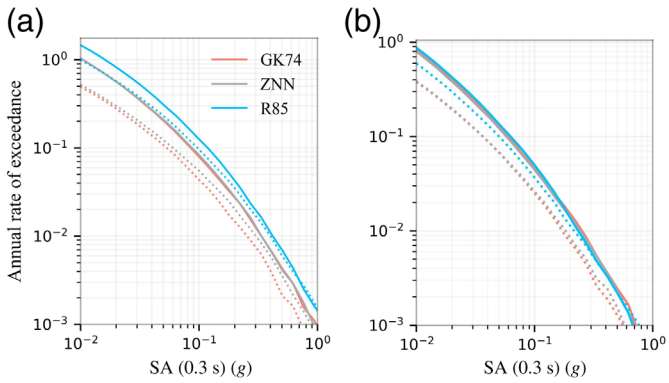

Figure 8. Annual rate of exceedance for (a) Norcia and (b) Perugia. The rates from the Omori model are shown with a solid line and those from the Poisson model with the dotted line. Random initial conditions are assumed, that is, the "unconditional" case. The color version of this figure is available only in the electronic edition.

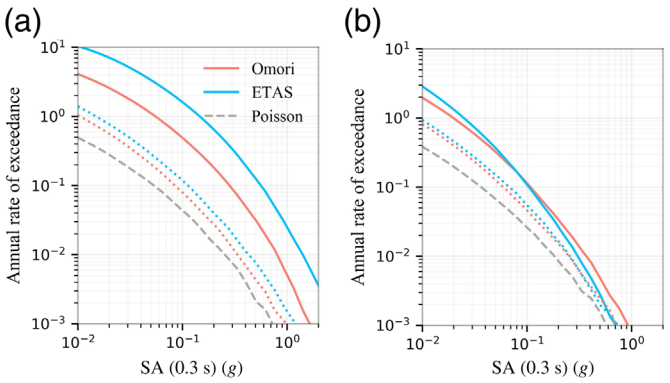

Figure 9. Annual rate of exceedance for (a) Norcia and (b) Perugia obtained using Omori and ETAS models. The conditional case (active ongoing sequences) is illustrated with a solid line and the unconditional case (average seismicity) with a dotted line. The color version of this figure is available only in the electronic edition.

earthquake. As explained in the Introduction, following Papadopoulos *et al.* (2020), we produce two sets of ETAS hazard estimates. In the first so-called "unconditional" case, we generate 11 yr of seismicity with no initial conditions (i.e., no auxiliary period), and we retain only the last simulated year. This procedure guarantees an unbiased seismicity level (i.e., neither high nor low compared to the long-term one) as the initial conditions for the catalogs used for hazard calculations. In the second so-called "conditional" model, the initial conditions are controlled and fixed to a specific auxiliary 2 year period and, again, the seismicity of the following year is simulated. Herein, as an auxiliary period, we choose the high-seismicity period 26 April 2015–26 April 2017 with active ongoing sequences, and we simulate the seismicity of 26 April 2017–26 April 2018.

For the Poisson + Omori model (in the following text, for brevity, we simply refer to this model as the Omori model), we also consider these two cases. The "unconditional case" is conceptually the same, whereas we feed the model with the seismicity observed in the auxiliary two-year-long initial window extracted this time from the declustered catalog in the "conditional" case, as, by definition, only mainshock events can generate aftershocks within this model. Naturally, as the Poisson model is time independent, there is no distinction between the "conditional" and "unconditional" cases. In all the hazard analysis computations, we only consider events with magnitude $\mathbf{M} \geq 4$. The seismic hazard curves are derived by counting the number of events that exceed each given level of spectral acceleration and dividing it by the total number of stochastic one-year-long catalogs, that is, annual rates are estimated. If the annual probabilities of one or more exceedances are needed, one needs to count the number of stochastic catalogs in which each given level of spectral acceleration is exceeded at least once and divide it by the total number of stochastic one-year-long catalogs simulated.

Poisson and Omori model comparison

In Figure 8, we compare the annual rate of exceedance of SA (0.3 s) obtained via both the Poisson and Omori models, considering the three different declustering techniques of GK74, R85, and ZNN. First, we can observe that the hazard estimates obtained with the Omori model are higher than those from the Poisson ones for all declustering methods and both considered sites, as expected, given that the rates are higher in the former case. The GK and ZNN models yield similar results for both the Poisson and Omori models and for both the sites. ZNN hazard estimates are slightly higher for larger intensities in the Poisson case, possibly due to the lower GR b-value that causes a higher rate of large-magnitude events.

R85 results in higher hazard estimates in the Poisson case for both Norcia and Perugia, which was expected, as the R85 declustered catalog contains more events (Fig. 5). On the other hand, in the Omori model, the difference is observed only for Norcia, for which R85 again predicts the highest hazard estimates, whereas the three curves are almost indistinguishable in Perugia. This might be due to the differences in the spatial distribution of the events in different Omori models, as R85 retains more events in the central part of the region, where Norcia is located (figures illustrating spatial distribution can be found in the supplemental material). One should remember that the earthquake occurrences in the R85 declustered catalog do not follow a Poisson distribution, and, hence, the obtained hazard curve is not coherent with the hypothesis.

Omori and ETAS model comparison

Figure 9 compares the Norcia and Perugia hazard curves produced by the Omori, ETAS, and Poisson models. For brevity, we only consider here Poisson and Omori model based on the GK74 declustered catalog. As expected, in all cases considered, both Omori and ETAS generate hazard curves that are

undoubtedly higher than the Poisson-based one. In the unconditional case, the annual rates found with the ETAS model are consistently higher than those found with the Omori model, although not significantly. This result implies that both the models are equally suitable to compute hazard in periods of average seismicity. However, in the conditional case, the year of hazard computations follows a period plagued by an active sequence. In this case, the ETAS results are considerably higher than those based on the Omori model. The reason for this is that 102 events with magnitude **M** ≥4 occurred in the investigated region in the auxiliary period used as initial conditions for the ETAS model. Only seven such events, which survived the declustering, are fed to the OMORI model. Some of the events removed by the declustering process are the high-magnitude events (**M** ≥5) that preceded and followed the **M** 6.6 mainshock earthquake that occurred on 30 October 2016 nearby Norcia. Based on the findings of this example, we infer that the Omori and ETAS model can predict significantly different results in periods of higher than average seismicity during ongoing active sequences.

The earlier statement, however, seems to apply only to sites close to the sequences. For Perugia, which is significantly farther from the focus of the activity, ETAS yields higher rates for lower intensities but lower rates for higher intensities. Hence, it is intuitive to expect that the Omori model may provide hazard estimation similar to the ETAS at sites away from the bulk of the active sequences, even in the period of heightened activity. These are only simple considerations, and more investigations should be conducted. However, it should be underlined that finding the reasons that may cause differences in the hazard estimates from ETAS and Omori models is anything but simple. Besides the apparent difference in how productivity and temporal distribution of aftershocks are modeled, their spatial distributions can also affect the hazard estimates. As described previously, the spatial distribution of background events in ETAS is estimated based on the declustered catalogs, whereas the distribution of triggered seismicity is described with an isotropic kernel without considering the fault geometry. In the Omori model, the spatial distribution of the aftershocks is modeled with a simple scaling law. The effect of these assumptions needs further investigation but is outside our study's scope.

DISCUSSION AND CONCLUSIONS

The objective of this study was threefold: (1) to estimate seismic hazard using the ETAS model, (2) to investigate the spatial variability of the ETAS parameters, and (3) to compare hazard estimates from ETAS with those based on Poisson and Omori models.

First, by comparing the MFD of the historical CPTI15 catalog with the MFD of the ETAS generated stochastic catalogs, we have shown that the ETAS model can adequately describe the past seismicity in the two considered regions in Italy. Furthermore, this study has shown that models based on the mainshock-only view of seismicity are often used, despite several limitations, leading to hazard estimates that are significantly lower compared to those obtained with more advanced tools capable of accounting for the triggered seismicity, such as the Omori or ETAS models. In addition, a PSHA approach based on the ETAS model for simulating future seismicity also appears to be able, unlike the Omori model, to capture the temporal variation in seismic hazard both in quiet and active periods of clustered seismicity.

The application of the ETAS model for seismic hazard estimation, however, is complex. There are many regions where an insufficient number of active sequences have occurred in the (short and recent) period of the earthquake catalog that can be considered as complete for lower magnitude events, as required by the method. Hence, our second objective was to investigate if it is legitimate to use ETAS parameters' values from a region well constrained by data and apply them elsewhere. We have defined two regions, Central Italy (region 1) and Southern Italy (region 2), and used the recent instrumental HORUS catalog, which covers the period from 1981 to 2020, to calibrate the ETAS model. We found that the parameter estimates are different for these two investigated regions with similar tectonic environments. However, at least, in the area considered, we can speculate that this discrepancy is more likely due to the scarcity of sequences in the observed period rather than to intrinsic differences in the earthquake sequence phenomena. Our conjecture is supported by comparing the MFDs for **M** 6+ events of 100 ETAS-simulated catalogs with the historical CPTI15 catalog covering the period from 1717 to 2017. These findings show a better agreement between simulated and observed frequency distributions when the more robust values of the ETAS clustering parameters from Central Italy are used to model sequences in the south, where sequences were scarce in the past few decades.

Finally, for the sake of comparison, we have examined the classical Poissonian model that considers mainshocks only, and the model that combines the Poissonian model for mainshocks and the modified Omori law for modeling aftershocks (Omori model), which is considered to be an approach for clustered seismicity modeling less complicated than ETAS. Because the Omori model is sensitive to the identification of mainshocks, we have investigated three different declustering methods, namely Gardner and Knopoff (1974), Reasenberg (1985), Zaliapin *et al.* (2008). We have found that these methods return catalogs with a different number of events, different *b*-values of GR law, different *p*-values of the K–S test for assessing the suitability of the Poisson distribution, different sets of Omori parameters' values, and an MFD not comparable to the observed one. Among the three, we favor GK74, which is the simplest and yields a catalog of events with occurrences distributed more closely to the Poisson distribution. We have investigated if the differences in the models described earlier significantly impact the hazard estimates, expressed in terms

of the annual rate of exceedance of ground-motion intensity measures at two sites in Central Italy. We have first compared the Omori and Poisson model, using the three different declustering methods. We have illustrated that the results might vary depending on the declustering method adopted. We then compared the three alternative models (Poisson, Omori, and ETAS) using two different initial conditions: an "unconditional" case, with initial conditions characterized by average seismicity, and a "conditional case," whose initial conditions included an ongoing active earthquake sequence. As expected, our findings indicate that the traditional Poissonian approach for earthquake occurrence modeling tends to provide lower hazard estimates. Considering aftershocks in the Omori model and all the events in the ETAS model significantly increases the hazard estimates to more realistic values because it does not account for the effect of the largest events only, like in the case of Poissonian approach. These promising results suggest the need to additionally investigate and improve the models used for describing spatiotemporal clustering. Furthermore, we have shown that the Omori and ETAS models yield similar hazard estimates during periods of average seismic activity for particular sites and intensity measure. However, during periods of increased activity, such as those following an active sequence, and for a site close to the sequence, the Omori model predicts lower hazard, because it is unable to consider the temporally varying hazard stemming from the heightened initial conditions.

There are several appealing features in the ETAS model: It incorporates the non-Poissonian nature of the earthquake occurrence phenomenon; it does not require the somewhat arbitrary classification of events into the mainshocks, foreshocks, and aftershocks; it relies on the GR law of the entire catalog circumventing the subjective choice of labeling mainshock, foreshocks, and aftershocks; it is adaptive; and it is well suited for performance-based methodology, as it does not neglect, unlike the Poisson and Omori models, any events that may increase the chance of observing certain levels of ground motions at a site. Although the use of the ETAS model for hazard computations is undoubtedly promising, several aspects of it can be improved. For example, fault geometry and anisotropic kernel for aftershock distribution, the time-varying magnitude of completeness, potential intersequence variability of the parameters, time-dependent background rate, and effect of the temporal and spatial window are some of the traits that deserve further investigation.

DATA AND RESOURCES

The HOmogenized instRUmental Seismic (HORUS) catalog can be downloaded at HORUS catalog (ingv.it). The parametric catalog of Italian earthquakes CPTI15 is available at CPTI15-DBMI15 v2.0 (ingv.it). All websites were last accessed in December 2020. The supplemental material includes the estimation of epidemic-type aftershock sequence (ETAS) parameters using different auxiliary temporal windows, additional Turing tests (10-day seismicity rate, spatial distribution, and aftershock productivity), spatial distribution maps of events in different declustered catalogs, and spatial distribution maps of events in stochastic catalogs generated with the Omori and ETAS models.

DECLARATION OF COMPETING INTERESTS

The authors declare that there are no competing interests.

ACKNOWLEDGMENTS

The authors want to thank Associate Editor Delphine D. Fitzenz, Andy Michael, and the anonymous reviewer for valuable comments that improved the article. The first, second, and fifth authors would like to acknowledge the funding provided through the MEthods and Tools' Innovation for Seismic safety assessment (METIS project: METIS—Seismic Risk Assessment for Nuclear Safety available at metis-h2020.eu, last accessed January 2022). The METIS project has received funding from the Horizon 2020 programme under Grant Agreement n°945121.

REFERENCES

Abrahamson, N. A., W. J. Silva, and R. Kamai (2014). Summary of the ASK14 ground motion relation for active crustal regions, *Earthq. Spectra* **30,** no. 3, 1025–1055, doi: 10.1193/070913EQS198M.

Aki, K. (1965). Maximum likelihood estimate of b in the formula log N = a–bM and its confidence limits, *Bull. Earthq. Res. Inst. Tokyo Univ.* **43,** 237–239.

Boyd, O. S. (2012). Including foreshocks and aftershocks in time-independent probabilistic seismic-hazard analyses, *Bull. Seismol. Soc. Am.* **102,** no. 3, 909–917, doi: 10.1785/0120110008.

Chu, A., F. P. Schoenberg, P. Bird, D. D. Jackson, and Y. Y. Kagan (2011). Comparison of ETAS parameter estimates across different global tectonic zones, *Bull. Seismol. Soc. Am.* **101,** no. 5, 2323–2339, doi: 10.1785/0120100115.

Console, R., M. Murru, and A. M. Lombardi (2003). Refining earthquake clustering models, *J. Geophys. Res.* **108,** no. B2, doi: 10.1029/2002JB002130.

Dascher-Cousineau, K., E. E. Brodsky, T. Lay, and T. H. W. Goebel (2020). What controls variations in aftershock productivity? *J. Geophys. Res.* **125,** no. 2, doi: 10.1029/2019JB018111.

Felzer, K. R., R. E. Abercrombie, and G. Ekström (2003). Secondary aftershocks and their importance for aftershock forecasting, *Bull. Seismol. Soc. Am.* **93,** no. 4, 1433–1448, doi: 10.1785/0120020229.

Field, E. H., and K. R. Milner (2018). Candidate products for operational earthquake forecasting illustrated using the haywired planning scenario, including one very quick (and not-so-dirty) hazard-map option, *Seismol. Res. Lett.* **89,** no. 4, 1420–1434, doi: 10.1785/0220170241.

Field, E. H., R. J. Arrowsmith, G. P. Biasi, P. Bird, T. E. Dawson, K. R. Felzer, D. D. Jackson, K. M. Johnson, T. H. Jordan, C. Madden, *et al.* (2014). Uniform California earthquake rupture forecast, version 3 (UCERF3)—The time-independent model, *Bull. Seismol. Soc. Am.* **104,** no. 3, 1122–1180, doi: 10.1785/0120130164.

Fitzenz, D., and C. Langenbruch (2021). A three kernel approach to earthquake source modeling: Incorporating incomplete or low resolution seismicity, fault and deformation datasets in continental China, *Annual Meeting of the Seismological Society of America 2021*, April 2021.

Frankel, A. (1995). Mapping seismic hazard in the central and eastern United States, *Seismol. Res. Lett.* **66,** no. 4, 8–21, doi: 10.1785/gssrl.66.4.8.

Gardner, J. K., and L. Knopoff (1974). Is the sequence of earthquakes in southern California with aftershocks removed, Poissonian? *Bull. Seismol. Soc. Am.* **64,** no. 5, 1363–1367.

Gee, R., L. Peruzza, and M. Pagani (2021). The power of the little ones: Computed and observed aftershock hazard in central Italy, *Earthq. Spectra* doi: 10.1177/87552930211036913.

Hainzl, S., G. B. Brietzke, and G. Zöller (2010). Quantitative earthquake forecasts resulting from static stress triggering, *J. Geophys. Res.* **115,** no. B11, doi: 10.1029/2010JB007473.

Hainzl, S., O. Zakharova, and D. Marsan (2013). Impact of aseismic transients on the estimation of aftershock productivity parameters, *Bull. Seismol. Soc. Am.* **103,** no. 3, 1723–1732, doi: 10.1785/0120120247.

Hardebeck, J. L., A. L. Llenos, A. J. Michael, M. T. Page, and N. van der Elst (2019). Updated California aftershock parameters, *Seismol. Res. Lett.* **90,** no. 1, 262–270, doi: 10.1785/0220180240.

Iervolino, I., M. Giorgio, and B. Polidoro (2014). Sequence-based probabilistic seismic hazard analysis, *Bull. Seismol. Soc. Am.* **104,** no. 2, 1006–1012, doi: 10.1785/0120130207.

Lilliefors, H. W. (1969). On the Kolmogorov-Smirnov test for the exponential distribution with mean unknown, *J. Am. Stat. Assoc.* **64,** no. 325, 387–389.

Llenos, A. L., and A. J. Michael (2020). Regionally optimized background earthquake rates from ETAS (Robere) for probabilistic seismic hazard assessment, *Bull. Seismol. Soc. Am.* **110,** no. 3, 1172–1190, doi: 10.1785/0120190279.

Lolli, B., D. Randazzo, G. Vannucci, and P. Gasperini (2020). The Homogenized Instrumental Seismic catalog (HORUS) of Italy from 1960 to present, *Seismol. Res. Lett.* **91,** no. 6, 3208–3222, doi: 10.1785/0220200148.

Lombardi, A. M. (2017). The epistemic and aleatory uncertainties of the ETAS-type models: An application to the central Italy seismicity, *Sci. Rep.* **7,** doi: 10.1038/s41598-017-11925-3.

Lombardi, A. M., and W. Marzocchi (2007). Evidence of clustering and nonstationarity in the time distribution of large worldwide earthquakes, *J. Geophys. Res.* **112,** doi: 10.1029/2006JB004568.

Luen, B., and P. B. Stark (2012). Declustering and poisson tests, *Geophys. J. Int.* **189,** no. 1, 691–700.

Marsan, D., and A. Helmstetter (2017). How variable is the number of triggered aftershocks? *J. Geophys. Res.* **122,** no. 7, 5544–5560, doi: 10.1002/2016JB013807.

Marzocchi, W., and M. Taroni (2014). Some thoughts on declustering in probabilistic seismic-hazard analysis, *Bull. Seismol. Soc. Am.* **104,** no. 4, 1838–1845, doi: 10.1785/0120130300.

Marzocchi, W., I. Spassiani, A. Stallone, and M. Taroni (2020). How to be fooled searching for significant variations of the b-value, *Geophys. J. Int.* **220,** no. 3, 1845–1856, doi: 10.1093/gji/ggz541.

Meletti, C., W. Marzocchi, V. D'Amico, G. Lanzano, L. Luzi, F. Martinelli, B. Pace, A. Rovida, M. Taroni, F. Visini, *et al.* (2021). The new Italian seismic hazard model (MPS19), *Ann. Geophys.* doi: 10.4401/ag-8579.

Mizrahi, L., S. Nandan, and S. Wiemer (2021). The effect of declustering on the size distribution of mainshocks, *Seismol. Res. Lett.* **92,** no. 4, 2333–2342, doi: 10.1785/0220200231.

Molchan, G. M., and O. E. Dmitrieva (1992). Aftershock identification: Methods and new approaches, *Geophys. J. Int.* **109,** no. 3, 501–516, doi: 10.1111/j.1365-246X.1992.tb00113.x.

Nandan, S., G. Ouillon, S. Wiemer, and D. Sornette (2017). Objective estimation of spatially variable parameters of epidemic type aftershock sequence model: Application to California, *J. Geophys. Res.* **122,** no. 7, 5118–5143, doi: 10.1002/2016JB013266.

Ogata, Y. (1988). Statistical models for earthquake occurrences and residual analysis for point processes, *Am. Stat. Assoc.* **83,** no. 401, 9–27.

Ogata, Y. (1998). Space-time point-process models for earthquake occurrences, *Ann. Inst. Stat. Math.* **50,** no. 2, 379–402.

Ogata, Y., and J. Zhuang (2006). Space-time ETAS models and an improved extension, *Tectonophysics* **413,** nos. 1/2, 13–23, doi: 10.1016/j.tecto.2005.10.016.

Omori, F. (1894). On the aftershocks of earthquake, *J. Coll. Sci. Imp. Univ. Tokyo* **7,** 111–200.

Pagani, M., D. Monelli, G. Weatherill, L. Danciu, H. Crowley, V. Silva, P. Henshaw, L. Butler, M. Nastasi, L. Panzeri, *et al.* (2014). OpenQuake Engine : An open hazard (and risk) software for the global earthquake model, *Seismol. Res. Lett.* **85,** no. 3, 692–702, doi: 10.1785/0220130087.

Page, M. T., and N. J. van Der Elst (2018). Turing-style tests for UCERF3 synthetic catalogs, *Bull. Seismol. Soc. Am.* **108,** no. 2, 729–741, doi: 10.1785/0120170223.

Page, M. T., N. van Der Elst, J. Hardebeck, K. Felzer, and A. J. Michael (2016). Three ingredients for improved global aftershock forecasts: Tectonic region, time-dependent catalog incompleteness, and intersequence variability, *Bull. Seismol. Soc. Am.* **106,** no. 5, 2290–2301, doi: 10.1785/0120160073.

Papadopoulos, A. N., P. Bazzurro, and W. Marzocchi (2020). Exploring probabilistic seismic risk assessment accounting for seismicity clustering and damage accumulation: Part I. Hazard analysis, *Earthq. Spectra* **37,** no. 2, doi: 10.1177/8755293020957338.

Peresan, A., and S. Gentili (2020). Identification and characterisation of earthquake clusters: A comparative analysis for selected sequences in Italy and adjacent regions, *Boll. Geof. Teor. Appl.* **61,** no. 1, 57–80, doi: 10.4430/bgta0249.

Petersen, M. D., M. Eeri, A. M. Shumway, P. M. Powers, M. Eeri, C. S. Mueller, M. P. Moschetti, M. Eeri, A. D. Frankel, M. Eeri, *et al.* (2020). The 2018 update of the US national seismic hazard model: Overview of model and implications, *Earthq. Spectra* **36,** no. 1, 5–41, doi: 10.1177/8755293019878199.

Reasenberg, P. (1985). Second-order moment of central california seismicity, 1969–1982, *J. Geophys. Res.* **90,** 5479–5495.

Reasenberg, P. A., and L. M. Jones (1989). Earthquake hazard after a mainshock in California, *Science*, **243,** no. 4895, 1173–1176.

Rovida, A., M. Locati, R. Camassi, B. Lolli, and P. Gasperini (2020). The Italian earthquake catalogue CPTI15, *Bull. Earthq. Eng.* **18,** 2953–2984.

Savage, W. U. (1972). Microearthquake clustering near Fairview Peak, Nevada, and in the Nevada seismic zone, *J. Geophys. Res.* **77,** no. 35, 7049–7056, doi: 10.1029/JB077i035p07049.

Seif, S., A. Mignan, J. D. Zechar, M. J. Werner, and S. Wiemer (2017). Estimating ETAS: The effects of truncation, missing data, and model assumptions, *J. Geophys. Res.* **122,** no. 1, 449–469, doi: 10.1002/2016JB012809.

Shome, N., and C. Williams (2014). Aftershock risk in Japan following Tohoku earthquake, *Proc. of the 10th National Conf. in Earthquake Engineering, Earthquake Engineering Research Institute*, Anchorage, Alaska, 21–25 July 2014.

Spassiani, I., and W. Marzocchi (2018). How likely does an aftershock sequence conform to a single omori law behavior? *Seismol. Res. Lett.* **89,** no. 3, 1118–1128, doi: 10.1785/0220170224.

Stallone, A., and W. Marzocchi (2019). Features of seismic sequences are similar in different crustal tectonic regions, *Bull. Seismol. Soc. Am.* **109,** no. 5, 1594–1604, doi: 10.1785/0120180175.

Taroni, M., and A. Akinci (2021). Good practices in PSHA: Declustering, b-value estimation, foreshocks and aftershocks inclusion; A case study in Italy, *Geophys. J. Int.* **224,** no. 2, 1174–1187, doi: 10.1093/gji/ggaa462.

Taroni, M., W. Marzocchi, D. Schorlemmer, M. J. Werner, S. Wiemer, J. D. Zechar, L. Heiniger, and F. Euchner (2018). Prospective CSEP evaluation of 1-day, 3-month, and 5-yr earthquake forecasts for Italy, *Seismol. Res. Lett.* **89,** no. 4, 1251–1261, doi: 10.1785/0220180031.

Teng, B. G., and J. W. Baker (2019). Seismicity declustering and hazard analysis of the Oklahoma–Kansas region, *Bull. Seismol. Soc. Am.* **109,** no. 6, 2356–2366, doi: 10.1785/0120190111.

Utsu, T. (1961). A statistical study on the occurrence of aftershocks, *Geophys. Mag.* **30,** 521–605.

Utsu, T. (1966). A statistical significance test of the difference in b-value between two earthquake groups, *J. Phys. Earth* **14,** no. 2, 37–40.

Utsu, T., and Y. Ogata (1995). The centenary of the omori formula for a decay law of aftershock activity, *J. Phys. Earth* **43,** no. 1, 1–33, doi: 10.4294/jpe1952.43.1.

van Stiphout, T., J. Zhuang, D. Marsan, S. S. Service, and E. T. H. Zurich (2012). Theme V—Models and techniques for analyzing seismicity, seismicity declustering, 1–25 February, doi: 10.5078/corssa-52382934.

Wang, Q., D. D. Jackson, and J. Zhuang (2010). Missing links in earthquake clustering models, *Geophys. Res. Lett.* **37,** no. 21, doi: 10.1029/2010GL044858.

Wang, Q., F. P. Schoenberg, and D. D. Jackson (2010). Standard errors of parameter estimates in the ETAS model, *Bull. Seismol. Soc. Am.* **100,** no. 5, 1989–2001, doi: 10.1785/0120100001.

Wells, D. L., and K. J. Coppersmith (1994). New empirical relationships among magnitude, rupture length, rupture width, rupture area, and surface displacement, *Bull. Seismol. Soc. Am.* **84,** no. 4, 974–1002.

Woessner, J., and S. Wiemer (2005). Assessing the quality of earthquake catalogues: Estimating the magnitude of completeness and its uncertainty, *Bull. Seismol. Soc. Am.* **95,** 684–698.

Wiemer, S. (2000). Introducing probabilistic aftershock hazard mapping, *Geophys. Res. Lett.* **27,** no. 20, 3405–3408, doi: 10.1029/2000GL011479.

Yeo, G. L., and C. A. Cornell (2009). A probabilistic framework for quantification of aftershock ground-motion hazard in California : Methodology and parametric study, *Earthq. Eng. Struct. Dynam.* **38,** 45–60, doi: 10.1002/eqe.840.

Zaliapin, I., and Y. Ben-Zion (2016). A global classification and characterization of earthquake clusters, *Geophys. J. Int.* **207,** no. 1, 608–634, doi: 10.1093/gji/ggw300.

Zaliapin, I., and Y. Ben-Zion (2020). Earthquake declustering using the nearest-neighbor approach in space-time-magnitude domain, *J. Geophys. Res.* **125,** no. 4, doi: 10.1029/2018jb017120.

Zaliapin, I., A. Gabrielov, V. Keilis-Borok, and H. Wong (2008). Clustering analysis of seismicity and aftershock identification, *Phys. Rev. Lett.* **101,** nos. 1/4, doi: 10.1103/PhysRevLett.101.018501.

Zhang, L., M. J. Werner, and K. Goda (2020). Variability of ETAS parameters in global subduction zones and applications to mainshock—Aftershock hazard assessment, *Bull. Seismol. Soc. Am.* **110,** no. 4, 191–212, doi: 10.1785/0120190121.

Zhuang, J., Y. Ogata, and D. Vere-Jones (2004). Analyzing earthquake clustering features by using stochastic reconstruction, *J. Geophys. Res.* **109,** no. 5, 1–17, doi: 10.1029/2003JB002879.

Zhuang, J., Y. Ogata, and T. Wang (2017). Data completeness of the Kumamoto earthquake sequence in the JMA catalog and its influence on the estimation of the ETAS parameters, *Earth Planets Space* **69,** no. 1, 1–12, doi: 10.1186/s40623-017-0614-6.

Zhuang, J., M. J. Werner, and D. S. Harte (2013). Stability of earthquake clustering models : Criticality and branching ratios, *Phys. Rev. E* **88,** no. 6, doi: 10.1103/PhysRevE.88.062109.

Manuscript received 4 August 2021
Published online 3 March 2022